Title

Biomimetic stochastic topography and electric fields synergistically enhance directional migration of corneal epithelial cells in a MMP-3-dependent manner

Journal

Acta Biomaterialia, 12(1)

ISSN

1742-7061

Authors

Gao, Jing

Raghunathan, Vijay Krishna

Reid, Brian

et al.

Publication Date

2015

DOI

10.1016/j.actbio.2014.10.007

Acta Biomaterialia 12 (2015) 102–112

Contents lists available at ScienceDirect

Acta Biomaterialia

journal homepage: www.elsevier.com/locate/actabiomat

Biomimetic stochastic topography and electric fields synergistically enhance directional migration of corneal epithelial cells in a MMP-3-dependent manner

Jing Gao [a,b,1], Vijay Krishna Raghunathan [c,1], Brian Reid [a], Dongguang Wei [d], Rodney C. Diaz [d], Paul Russell [c], Christopher J. Murphy [c,e,*], Min Zhao [a,b,e,*]

[a] Department of Dermatology, School of Medicine, University of California Davis, Sacramento, CA 95817, USA
[b] School of Life Science, Yunnan Normal University, Kunming, Yunnan 650500, People's Republic of China
[c] Department of Surgical and Radiological Sciences, School of Veterinary Medicine, University of California Davis, Davis, CA 95616, USA
[d] Department of Otolaryngology, School of Medicine, University of California Davis, Sacramento, CA 95817, USA
[e] Department of Ophthalmology & Vision Science, School of Medicine, University of California Davis, Sacramento, CA 95817, USA

ARTICLE INFO

Article history:
Received 9 June 2014
Received in revised form 2 October 2014
Accepted 4 October 2014
Available online 13 October 2014

Keywords:
Electric field
Topography
Basement membrane
Corneal epithelial cells
Cornea

ABSTRACT

Directed migration of corneal epithelial cells (CECs) is critical for maintenance of corneal homeostasis as well as wound healing. Soluble cytoactive factors and the intrinsic chemical attributes of the underlying extracellular matrix (ECM) participate in stimulating and directing migration. The central importance of the intrinsic biophysical attributes of the microenvironment of the cell in modulating an array of fundamental epithelial behaviors including migration has been widely documented. Among the best measures of these attributes are the intrinsic topography and stiffness of the ECM and electric fields (EFs). How cells integrate these multiple simultaneous inputs is not well understood. Here, we present a method that combines the use of (i) topographically patterned substrates (mean pore diameter 800 nm) possessing features that approximate those found in the native corneal basement membrane; and (ii) EFs (0–150 mV mm^{-1}) mimicking those at corneal epithelial wounds that the cells experience in vivo. We found that topographic cues and EFs synergistically regulated directional migration of human CECs and that this was associated with upregulation of matrix metalloproteinase-3 (MMP3). MMP3 expression and activity were significantly elevated with 150 mV mm^{-1} applied-EF while MMP2/9 remained unaltered. MMP3 expression was elevated in cells cultured on patterned surfaces against planar surfaces. The highest single-cell migration rate was observed with 150 mV mm^{-1} applied EF on patterned and planar surfaces. When cultured as a confluent sheet, EFs induced collective cell migration on stochastically patterned surfaces compared with dissociated single-cell migration on planar surfaces. These results suggest significant interaction of biophysical cues in regulating cell behaviors and will help define design parameters for corneal prosthetics and help to better understand corneal wound healing.

1. Introduction

The anterior corneal surface is covered by a stratified epithelial layer that is intimately associated with a rich 3-D topographically patterned specialization of the extracellular matrix (ECM), the anterior corneal basement membrane (BM). Primary functions of the corneal epithelium include protecting the eye from external physical, chemical and biological irritants, and providing a barrier to microbial invasion by maintaining a protective junctional barrier. Wounding of the epithelium results in loss of barrier function. Directed cell migration of epithelial cells is a critical process in wound healing. This involves interaction of epithelial cells with the BM promoting cell adhesion and migration into the wound [1] as well as coordinated responses to a multitude of soluble biochemical cues that create chemotactic gradients [2,3]. Matrix metalloproteinases (MMPs) also participate in coordinated movement of cells and matrix dynamics essential to wound repair processes.

Recent reports document another important and distinct class of factors for regulating migration of corneal epithelial cells (CECs) – namely biophysical cues intrinsic to the microenvironment of cells. Of these, among the best characterized are surface topography, substratum stiffness and electric fields (EFs). The cellular

* Corresponding authors at: Department of Ophthalmology & Vision Science, School of Medicine, University of California Davis, Sacramento, CA 95817, USA.
E-mail addresses: cjmurphy@ucdavis.edu (C.J. Murphy), minzhao@ucdavis.edu (M. Zhao).
[1] These authors contributed equally to this work.

http://dx.doi.org/10.1016/j.actbio.2014.10.007
1742-7061/

response to biophysical cues is an increasingly important component of biomaterials design and as a factor for studying cell differentiation, changes in gene and protein expression, and wound healing. Corneal epithelial cells respond to substratum anisotropically ordered topographic cues by aligning parallel or perpendicular to the ridges and grooves, responses that are strongly influenced by the size scale of the topographic features [4–8]. Soluble factors [9], and coating with RGD peptides [10–12] and other ECM proteins [13], can alter the extent of corneal cell alignment and migration in response to the topographic cues. The use of anistropically ordered substrates of ridges and grooves mimics one feature type, i.e. fibers, of the BM and provides a rapid readout of cellular alignment response. However, it has been demonstrated that the BM is a more three-dimensionally complex structure with topographic features having stochastic surface order on the nano- and submicron size-scale (50–500 nm) [14–20]. Here we report the use of biomimetic, stochastically ordered substrates to best approximate the features characteristic of the anterior corneal BM, and use these to determine the interaction of topographic cues with EFs in modulating CEC migration.

The responses of plant and animal cells to applied EFs were first studied over a century ago. In 1780, Luigi Galvani discovered that the muscles of dead frogs twitched when stimulated with an electric spark [21]. Wilhelm Roux in 1892 applied EFs to a variety of animal eggs and observed stratifications of the cytoplasm [22]. The experimental techniques were later improved to use a more physiological EF and minimize artifacts such as pH changes. Indeed, cell migration in response to EFs (electrotaxis) was documented much later. In the presence of an applied EF, many cell types, including neurons, neural crest cells, fibroblasts and others, migrate to the cathode [23–27]. Our laboratory and others have demonstrated that CECs and keratocytes, cultured on standard plasticware, migrate to the cathode in physiological EFs [28–32]. The corneal epithelium actively pumps ions to generate an electrical transepithelial potential (TEP). Corneal injury rapidly induces large EFs and currents. CECs use these electric signals as a directional cue to guide them into the wound. Endogenous EFs at the site of the wound are a stimulus equally as potent as soluble factors in directing cell migration [33]. Indeed, in the cornea, there is a strong correlation between wound electrical activity and the rate of wound healing [34]. In fact, Chiang and co-workers measured EFs of the order of 42 mV mm^{-1} near the wound edge on the surface of isolated bovine eyes [35]. In mice and human skin, bioelectric fields of the order of 177 mV mm^{-1} have been measured [36]. While wound currents of 4.3 μA cm^{-2} were reported previously by our group in *ex vivo* rat corneal wounds [34], recent measurements of corneal wound current in live anesthetized rats in vivo were almost six times higher at 24.8 μA cm^{-2} (unpublished data). For all experiments described in this study, we conservatively use 150 mV mm^{-1} as our larger EF strength.

The impact of simultaneous presentation of biomimetic topographic cues and physiological EFs on CEC migration, and activity and expression of MMPs is unknown. In this study we cultured CECs on topographically patterned substrates possessing features that mimicked those intrinsic to the native BM while simultaneously providing EFs similar to those naturally detected at corneal wounds. We found these two biophysical cues to cooperatively regulate directional migration of human CECs. This migration occurred in association with upregulation of matrix metalloproteinase-3 (MMP3).

2. Materials and methods

Unless otherwise stated, chemicals and reagents were obtained from Sigma Aldrich, St Louis, MO.

2.1. Cell culture

Immortalized human CECs (hTCEpi) [37], kindly provided by Dr James V. Jester (University of California, Irvine), were maintained at 37 °C, 5% CO_2, in Epilife® medium (Invitrogen, Carlsbad, CA) supplemented with Epilife® defined growth supplement (EDGS, Invitrogen, Carlsbad, CA) and 1% penicillin/streptomycin (Gibco, Carlsbad, CA) and were used between passages 40 and 60. The medium was changed every 2 days. All experiments were repeated in triplicate.

2.2. Fabrication of stochastically ordered topographically patterned polymeric substrates

Polymeric substrates with stochastically ordered topography were fabricated as described previously [38]. Briefly, stochastically patterned master substrates were fabricated by forming phase-resolved and crosslinked polyelectrolyte multilayers (PEMs) of poly(acrylic acid) and poly(allylamine hydrochloride) on silanized glass slides (silanization was performed using 3-aminopropyltrimethoxysilane; Sigma Aldrich, St Louis, MO)). High-fidelity replicates of these nanotopographic features were created using a composite stamp of hard and thin polydimethylsiloxane (PDMS) and were designated as "master stamps". Using these master stamps, the patterns were replicated onto a thin layer of NOA81 optical adhesive (Norland Products, Cranbury, NJ) that had been coated across 60 or 100 mm tissue culture plates using a spin coater and cured in a XL-1500 UV cross-linker under 365 nm light for 100 min. NOA81, a proprietary mercaptoester compound of Norland Products, was supplied as a single-component liquid adhesive that readily cures as a rigid polymer with exposure to UV light. Research from our laboratory has previously documented NOA81 to be a suitable material for cell culture [39–41]. Fig. 1A shows the stochastically ordered topographically patterned substrate (mean pore diameter 800 nm) compared with the topographic features of the human corneal BM (pore diameter in the range of 50–500 nm [18]). To provide a relevant surface chemistry, we treated all polymeric substrates (planar and topographical) with a proprietary mixture of fibronectin–collagen (FNC). For this, immediately prior to cell seeding the surfaces were treated for 15 s with FNC coating mix (Athena Enzyme Systems, Baltimore, MD) as described previously [13]. Atomic force microscopic analysis confirmed that FNC coating did not alter the fidelity (roughness as measured by root mean square (RMS) values and pore diameter) of the topographic features (Fig. 1A).

2.3. Fabrication of electrotaxis chambers and application of EFs

All NOA81 substrates were sterilized by exposure to 280 nm UV light for 30 min in a laminar flow hood. Prior to cell seeding, a molecular coating of FNC (Athena Enzyme Systems, Baltimore, MD) was applied to all surfaces. Generation of physiological EFs to cells was accomplished as described in detail previously [42,43]. Electrotaxis chambers were made as shown in Fig. 1B. Cells (hTCEpi) were seeded at a density of 10,000 cells cm^{-2} onto flat or stochastic patterned NOA81 surfaces and allowed to settle and adhere for 2 h in an incubator at 37 °C and 5% CO_2. The electrotaxis chamber was connected to the power supply via 15 cm long agar-salt bridges (1.5% agar in Steinberg's solution) and beakers containing Steinberg's solution which also contained Ag/AgCl electrodes. Steinberg's solution contained: 58 mM NaCl, 0.67 mM KCl, 0.44 mM $Ca(NO_3)_2$, 0.3 mM $MgSO_4$, 4.6 mM Trizma base, pH 7.8–8.0. Cells were exposed to EFs with strength ranging from 25 to 150 mV mm^{-1} for 3 h at 37 °C with 5% CO_2. Field strengths were measured directly in the chamber at the beginning, in the middle

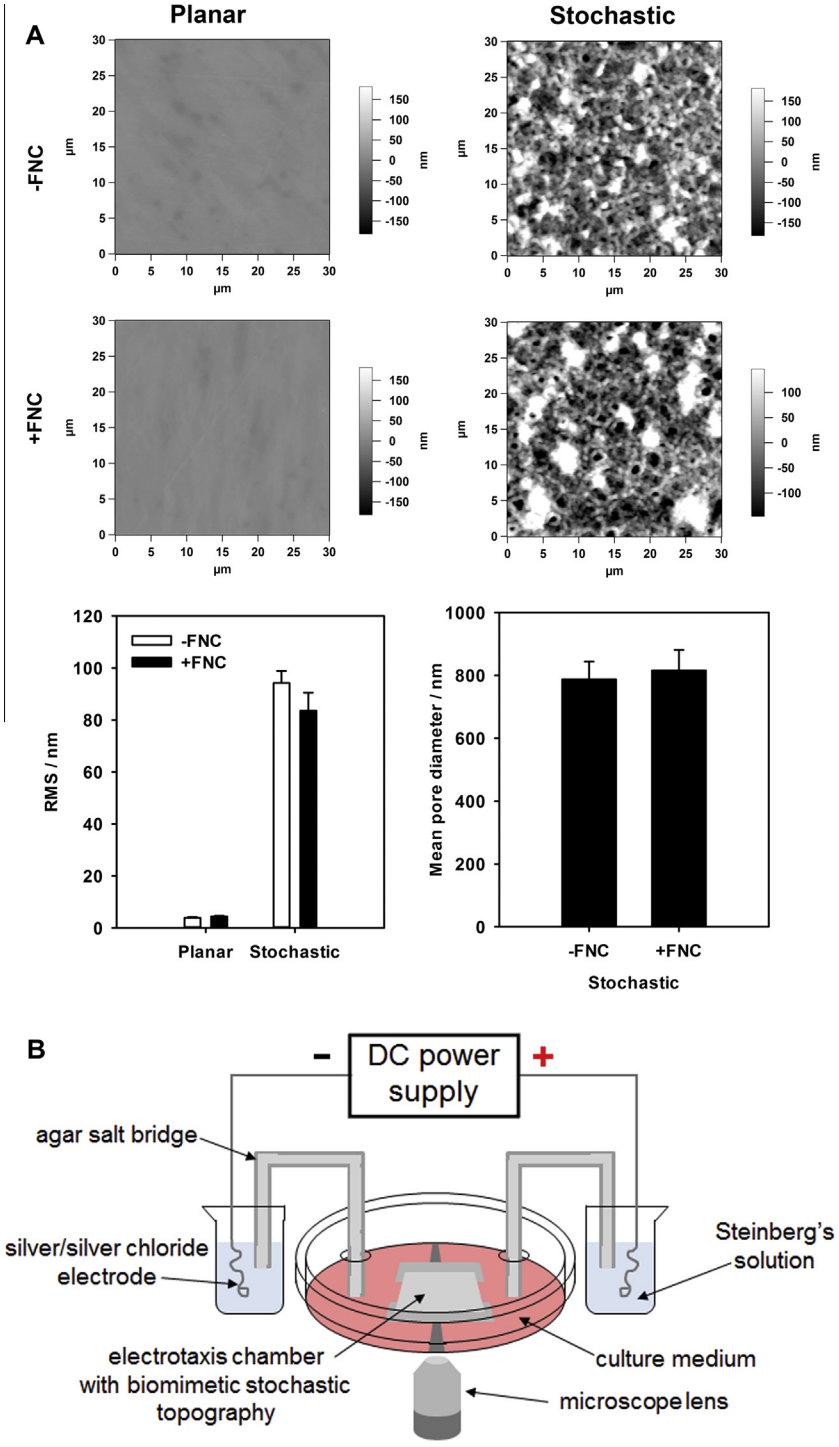

Fig. 1. Experimental setup that combines substratum topography and physiological EFs. (A) Atomic force microscopy (AFM) height images of planar and BM-like stochastic topography with or without fibronectin collagen (FNC) coating. Elevated root mean square (RMS) values demonstrate that stochastic topographies are "rougher" than planar surfaces. The mean pore diameter of the stochastic surfaces was ~800 nm. FNC coating did not appear to alter pore diameter or RMS values of the patterned surfaces. (B) Experimental setup to test cell electrotaxis. Cells were seeded into an electrotaxis chamber 1 cm wide × 2 cm long created by gluing two cover glasses to the base of the Petri dish. When the cells had adhered to the base the chamber was completed by placing a cover glass on top to create a narrow space through which the applied EF and current flows.

and the end of experiments. Phase-contrast timelapse images were taken using a Zeiss Axiovert 200M microscope with a Zeiss Axiocam HRm camera (Carl Zeiss, Oberkochen, Germany) at 10 min intervals at 10× magnification. Multiple fields of view were defined using Axiovision 4.6 software (Carl Zeiss, Germany) which also controlled the automated stage during image acquisition.

2.4. RNA isolation and quantitative real-time polymerase chain reaction (PCR) analyses for MMPs

To determine the mRNA expression levels of cells cultured on planar or topographically patterned surfaces, cells were harvested for RNA isolation 3 h after the application of EFs of 0, 25, 50 or

150 mV mm^{-1}. RNA was isolated using the RNeasy kit (Qiagen) following the manufacturer's instructions. Equal amounts of RNA (75 ng) were used for all real-time quantitative PCR (qPCR) reactions. Expression levels of MMP2, MMP3 and MMP9 were determined using the SensiFAST™ Probe Hi-ROX One-Step Kit (Bioline USA Inc, Taunton, MA) and aptamers specific to MMP2 (Hs00234422_m1), MMP3 (Hs00968380_m1) and MMP9 (Hs00234579_m1), all from Life Technologies. The reverse-transcription reaction was performed in a StepOne qPCR machine (Applied Biosystems/Life Technologies) with the following parameters: 30 min at 50 °C followed by 10 min at 95 °C; 40 cycles of 60 °C for 1 min followed by 95 °C for 15 s. Relative expression levels of the genes of interest were normalized to the expression of GAPDH (Hs99999905_m1; Life Technologies). Values for gene expression were normalized to mRNA level of the "no EF" samples, which were assigned a value of 1.0. The C_t values obtained represent logarithmic changes in gene expression. $\Delta\Delta C_t$ values between calibrator gene (GAPDH) and gene of interest (MMP2, etc.), normalized to the control sample ("no EF"), were calculated as described previously [44]. The experiment was performed in triplicate and repeated three times.

2.5. Protein isolation and Western blotting

Cell monolayers cultured on NOA81 surfaces were washed once in PBS and lysed and scraped into RIPA buffer (Thermo Scientific, Waltham, MA) supplemented with protease and phosphatase inhibitors (Fisher Scientific, Hampton, NH) on ice. The cells were homogenized and centrifuged at 1000*g* for 1 min to remove any cell debris. In order to quantify the expression of MMP3 secreted by cells, culture media was removed and used subsequently. Protein was quantified using a modified Lowry assay (DC assay, Bio-Rad, Hercules, CA) with bovine serum albumin as the standard. Protein homogenate/media supernatant was then denatured in Laemmli buffer (Sigma Aldrich, St Louis, MO) by boiling for 10 min. Approximately 10 μg protein per well were loaded for each sample. Protein was separated on NuPAGE® 10% Bis-Tris precast gels and transferred onto nitrocellulose membranes (both Life Technologies). Immunoblotting was done against anti-human MMP3 and β-actin (Abcam, Cambridge, MA) overnight at 4 °C. This was followed by incubation with secondary antibodies conjugated with horseradish peroxidase (HRP; Kirkegaard & Perry Laboratories, Gaithersburg, MD) for 1 h at 37 °C. Protein bands were detected by chemiluminescence using a WesternBright Quantum ECL detection kit (Advansta, CA). Blots were imaged using an ImageQuant 350 imaging system (GE Life Sciences). Densitometry analysis of the protein bands was performed using National Institutes of Health (NIH) ImageJ software (http://rsbweb.nih.gov/ij/) [45].

2.6. MMP3 immunocytochemistry

For labeling of MMP3, hTCEpi cells were fixed in 4% formaldehyde in phosphate-buffered saline (PBS; pH 7.4; 20 min), permeabilized in 0.1% Triton X-100 for 5 min, and blocked in a solution containing 20% goat serum and 1% bovine serum albumin (BSA) in PBS for 1 h. Cells were then incubated overnight at 4 °C with primary antibody specific to MMP3 (ab17790; Abcam, Cambridge, MA) in a solution containing 0.1% Triton X-100/1% BSA in PBS. Cells were washed three times with PBS and then incubated with goat anti-mouse secondary antibody conjugated with Cy3 (Jackson ImmunoResearch Laboratories, Inc., West Grove, PA) for 90 min at room temperature. Nuclei were counter-stained using DAPI (Life Technologies, Grand Island, NY). After a final wash, cells were mounted in Vectashield (Vector Laboratories, Inc., Burlingame, CA) under a cover glass. Fluorescent images were taken using the microscope described above (Section 2.3). All images were captured at the same exposure setting for each channel. Relative fluorescence was quantified after background subtraction using NIH ImageJ.

2.7. Quantification of MMP3 activity

MMP3 activity in the media supernatant and cell pellet was quantified using the Sensolyte® 520 MMP3 assay (ANASPEC, Fremont, CA) following the manufacturer's protocol. Briefly, pro-MMP was activated in the sample over 24 h at 37 °C by reacting with 4-aminophenylmercuric acetate (APMA). Equal volumes (50 μl) of pro-MMP3 activated sample and assay buffer were mixed together. Enzymatic reaction was initiated upon the addition of 50 μl MMP3 substrate solution. Relative changes in fluorescence were determined at 490 nm excitation/520 nm emission, every 5 min, for 60 min in a fluorescence spectrophotometer. The linear region over which a change in fluorescence was observed was used to determine enzyme activity. All reactions were performed against a known concentration of purified MMP3.

2.8. Cell migration analysis

NIH ImageJ software was used to quantify migration directedness and speed by tracing individual cells at frame intervals of 10 min. Only those cells that (i) did not move out of the field, (ii) did not contact other cells and (iii) did not divide during the course of the experiment were analyzed. Directedness ($\cos\theta$) was used to quantify the direction of cell migration, where θ is the angle between the field vector and the cell migration direction. Directedness is −1 if a cell migrates directly to the left (negative cathode), 0 if cell migrates perpendicular to the field direction, and +1 if a cell migrates directly to the right (positive anode). The equation $\sum i \cos\theta/N$ was used to calculate the cell population average directedness. Cell migration speed was quantified as trajectory speed and displacement speed; trajectory speed ($\mu m\ h^{-1}$) is the total migration distance divided by the time taken; displacement speed represents the straightline distance from startpoint to endpoint, divided by time taken (also in $\mu m\ h^{-1}$).

To monitor migration of confluent cell monolayers, a PDMS stopper (1 mm wide) was placed on planar or topographically patterned surfaces to create a cell-free analytic zone. Cells were seeded onto either side of the gasket at a cell density of 25,000 cells cm^{-2} and incubated overnight. Immediately prior to the application of EF/imaging, the gasket was removed, creating a cell-free "wound" space into which cells could migrate. Timelapse images were captured as above with an EF (150 mV) applied with the cathode to the right. Penetration of cells into the "wound" space was analyzed using NIH ImageJ by measuring the distance between adjacent pairs of cells at the wound edge at time zero and between the same cells 3 h after gasket removal (n = 18 pairs for both flat and stochastic). For experiments involving MMP3 inhibition, a 20 mM stock solution of MMP3 inhibitor (MMP3i; Santa Cruz Biotechnologies, CA, USA) was made in double-distilled water and diluted in growth medium to a final working concentration of 20 μM.

2.9. Statistical analyses

Data are presented as mean ± standard error of the mean (SEM). Comparisons of groups of cells with different treatments were done using Student's *t*-test/Mann–Whitney rank sum test, or ANOVA followed by Dunnett's multiple comparison/Dunn's pairwise comparison test as appropriate. Compared with corresponding control, significance is presented as: $^{*}P < 0.05$, $^{**}P < 0.01$, $^{***}P < 0.001$ (statistics labeled with a * symbol are results compared

with 0 mV mm^{-1} on stochastically pattered surfaces); $^{\#}P < 0.05$, $^{\#\#}P < 0.01$ $^{\#\#\#}P < 0.001$ (statistics labeled with a # symbol are results compared with 0 mV mm^{-1} on planar surfaces); $^{\&}P < 0.05$, $^{\&\&}P < 0.01$ and $^{\&\&\&}P < 0.001$ (statistics labeled with a & symbol are results comparing planar surfaces with stochastic surfaces).

3. Results

3.1. Electrotaxis of single cells on flat and topographically patterned surfaces

The direction of cellular migration was observed to be random in the absence of EFs on both topographically patterned and planar surfaces (Fig. 2A; traces show cell migration trajectories with the first position of each cell in the center). However, EFs of increasing strength stimulated migration towards the cathode (Fig. 2B–E; see also Supplementary movies 1–4). Cell directedness was enhanced as the field strength increased (Fig. 3A). With an EF strength of 150 mV mm^{-1} cell migration directedness was −0.943 ± 0.007 on flat surfaces (n = 180) and −0.925 ± 0.010 on stochastic surfaces (n = 303), which is close to the theoretical maximum of −1. An EF of 150 mV mm^{-1} induced significantly faster cell migration on topographically patterned surfaces compared with flat (Fig. 3B; $P < 0.001$). No significant differences in directedness of cell migration towards the cathode were observed between planar and topographically patterned surfaces ($P > 0.05$) at all field strengths tested (Fig. 3A). Cell migration rate was, however, significantly greater on topographically patterned surfaces than on planar surfaces for all EF strengths (Fig. 3B; 25 mV mm^{-1}, $P < 0.05$; 50 mV mm^{-1}, $P < 0.001$; 150 mV mm^{-1}, $P < 0.001$). Interestingly, reduced cell migration rates were observed on both surfaces in the presence of 25 and 50 mV mm^{-1} EF in comparison to 0 mV mm^{-1} EF, although migration rate was significantly elevated when an EF strength of 150 mV mm^{-1} was applied. In the presence of 150 mV mm^{-1} applied EF, cell migration speed was greatest, at 20.203 ± 0.649 μm h^{-1} on flat surfaces (n = 180), and 25.702 ± 0.575 μm h^{-1} on topographically patterned surfaces (n = 303) and this EF was thus chosen for monolayer migration assays.

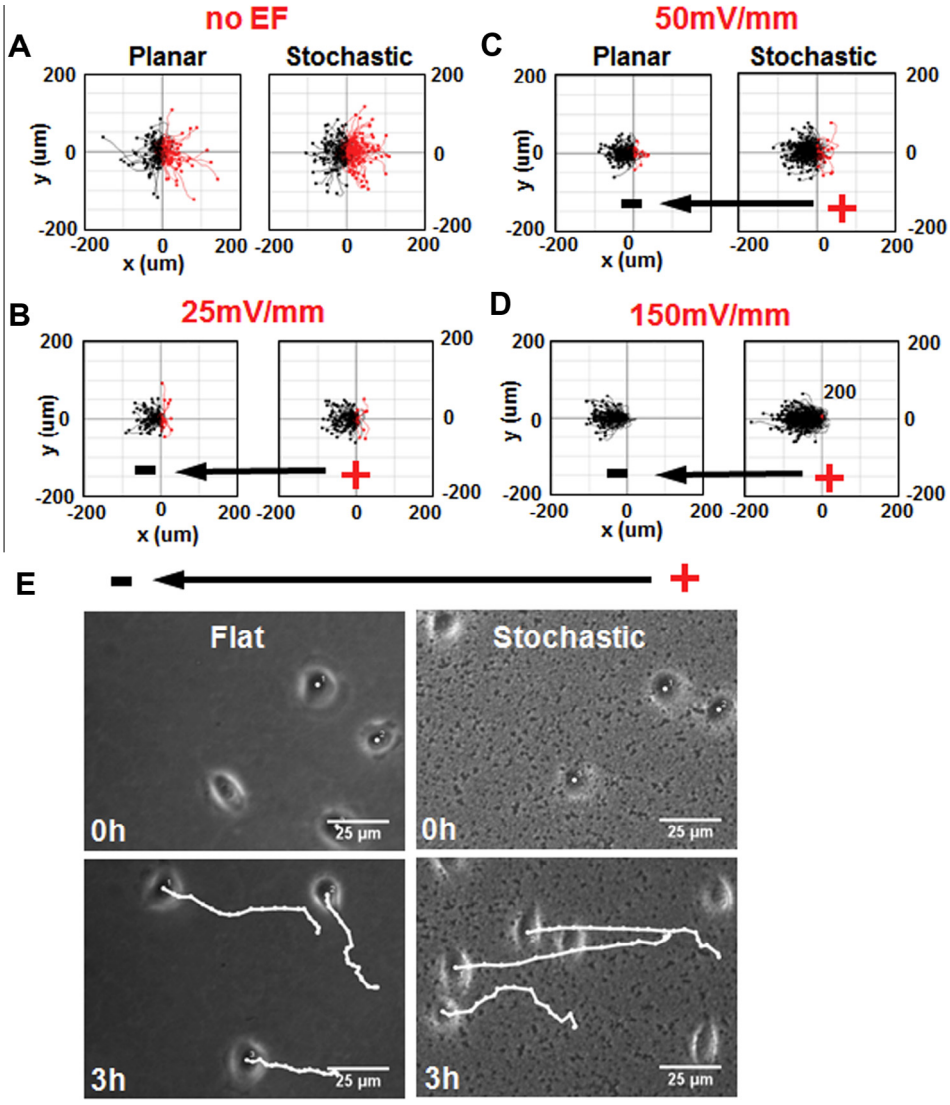

Fig. 2. Biomimetic stochastic topography and EFs synergistically enhance cell migration. (A) With no EF, cells on planar and stochastic surfaces migrated randomly. (B–D) Increasing EF strength induced cell migration to the cathode. Cell tracks to the left (black) = cathodal migration. Cell tracks to the right (red) = anodal migration. With increasing EF strength, migration on the stochastic surface appeared to be enhanced. (E) Sample images showing cells at time zero and after 3 h EF application on flat vs. stochastic surfaces. Cell tracks show the cell migration towards the cathode. Scale bars 25 μm. See also Supplementary movies 1–4.

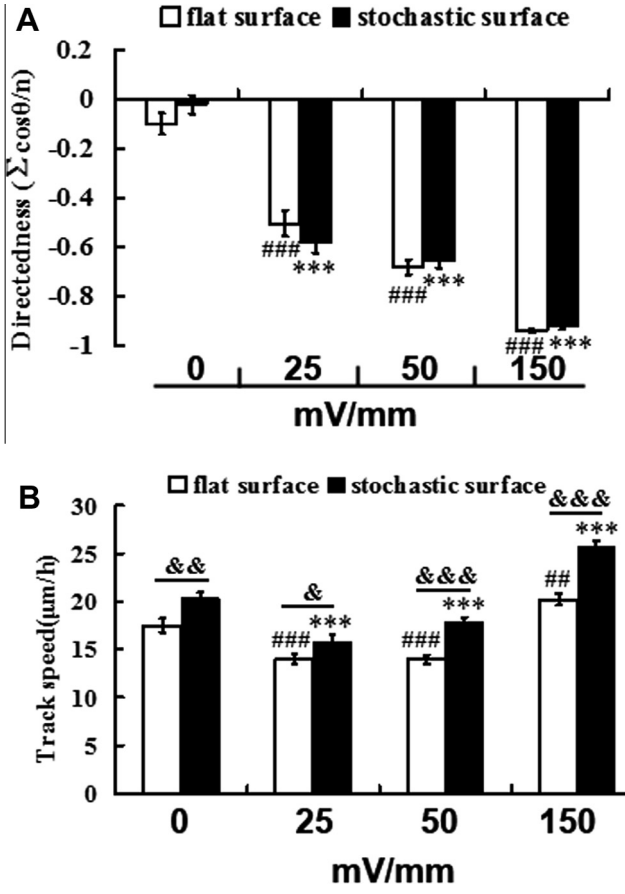

Fig. 3. Biomimetic stochastic topography and EFs synergistically enhance cell migration. (A) Cell migration directedness was enhanced with increasing EF strength but was not significantly different when comparing stochastic and planar surfaces. (B) In an EF of 150 mV mm^{-1} cell migration speed was significantly enhanced and was also significantly faster on stochastic compared to planar surfaces. All results are mean ± standard error: $^{*}P < 0.05$, $^{**}P < 0.01$, $^{***}P < 0.001$ (ANOVA followed by Dunnett's comparison, * are results compared with 0 mV mm^{-1} on stochastically patterned surfaces); $^{\#}P < 0.05$, $^{\#\#}P < 0.01$ ### (ANOVA followed by Dunnett's comparison, # are results compared with 0 mV mm^{-1} on planar surfaces); $^{\&}P < 0.05$, $^{\&\&}P < 0.01$ and $^{\&\&\&}P < 0.001$ (Mann–Whitney rank sum test, & are results comparing planar surfaces with stochastic surfaces under the same conditions).

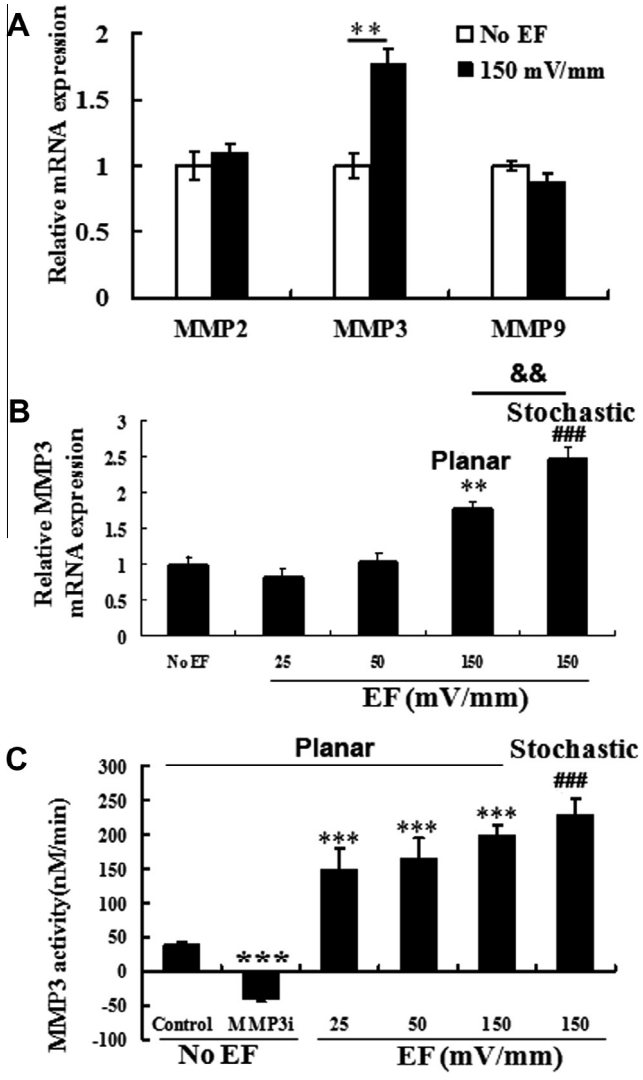

Fig. 4. Biomimetic stochastic topography and EFs specifically upregulated expression and activity of MMP3. (A) MMP3 (but not MMP2 or MMP9) expression (relative mRNA level) was significantly increased in human CECs after application of an EF of 150 mV mm^{-1} for 3 h ($^{**}P < 0.01$). (B) In an EF of 150 mV mm^{-1}, MMP3 expression was significantly enhanced on stochastic surface compared to flat ($^{**}P < 0.01$, $^{\#\#\#}P < 0.001$ compared with "no EF"; $^{\&\&}P < 0.01$ compared with planar). (C) MMP3 activity was increased in an EF- and surface-dependent manner. MMP3 inhibitor (MMP3i) significantly suppressed MMP3 activity ($^{***}P < 0.001$). Fluorescence profiles for the MMP3i and control groups were similar, although the actual fluorescence values for the MMP3i group were lower than those of control group, and thus appeared to be negative in activity.

3.2. Effect of applied EF on MMP gene expression

To determine the underlying molecular consequences of applying EFs to cells, changes in gene expression on planar surfaces in the presence or absence of EF was quantified by qPCR. Following EF application (3 h at 150 mV mm^{-1}) MMP3 expression level was significantly increased. The relative expression level was 2 times the control level (Fig. 4A; $P < 0.01$). The expression levels of MMP2 and MMP9 were not significantly different (comparing 150 mV mm^{-1} and no EF control; $P > 0.05$). As a consequence, we targeted MMP3 for further investigation.

3.3. MMP3 expression and activity

The influence of topographic cues on MMP3 expression and activity in the absence or presence of applied EFs was determined. MMP3 mRNA expression level remained unaltered in cells when EF strengths of 25 or 50 mV mm^{-1} were applied. However, with the application of a 150 mV mm^{-1} EF, MMP3 expression level was significantly increased (Fig. 4B). Intriguingly, expression of MMP3 was greater in cells cultured on topographically patterned surfaces compared with planar surfaces (Fig. 4B). Concurrently, MMP3 activity in the media supernatant was significantly elevated in an EF strength-dependent manner (Fig. 4C). MMP3 activity was also greater in the media supernatant of cells cultured on topographically patterned surfaces in comparison with planar surfaces. Specificity of MMP3 activity was confirmed by treatment of cells with 20 μM MMP3i (MMP3 inhibitor) which significantly inhibited MMP3 activity in the supernatant (Fig. 4C) although changes in MMP3 protein expression level were not observed (Fig. 5A).

As it was difficult to collect the lysate from cells cultured on patterned surfaces, we quantified MMP3 expression on planar surfaces. MMP3 expression was quantified in media supernatant and total cell lysate by immunocytochemistry and Western blotting. An EF strength-dependent increase in MMP3 expression was observed in total protein lysates (cell pellet), although no significant differences were observed in secreted MMP3 expression in the media supernatant (Fig. 5A and B). Additionally, treatment of

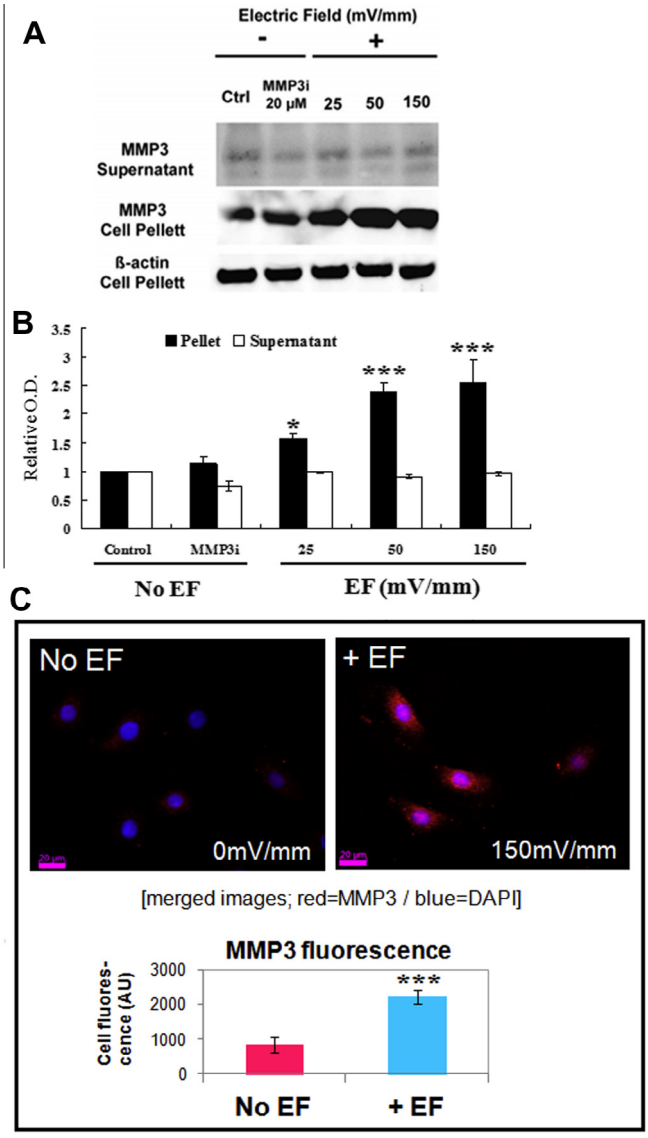

Fig. 5. Biomimetic stochastic surface and EFs specifically upregulated expression and activity of MMPs. (A and B) MMP3 protein expression was enhanced in an applied EF in the cells but not in the supernatant, indicating minimal secretion. Treatment of cells with 20 μM MMP3 inhibitor (MMP3i) did not significantly impair the expression of MMP3 in either supernatant or cell lysate ($^{*}P < 0.05$, $^{***}P < 0.001$). (C) Fluorescent labeling of MMP3 (red) shows upregulation of the protein after application of EF of 150 mV mm^{-1} for 3 h. Blue = DAPI labeling of DNA. Scale bars = 20 μm. Relative fluorescence intensity was also quantified from multiple images obtained and expressed as mean ± standard deviation (n = 10 locations).

cells with 20 μM MMP3 inhibitor (MMP3i) did not significantly impair the expression of MMP3 in either supernatant or cell lysate (Fig. 5B). Immunocytochemistry results revealed that while expression of MMP3 was elevated in the presence of an applied EF, its subcellular distribution was generally uniform and not preferentially aligned towards the cathode (Fig. 5C).

3.4. Electrotaxis of individual cells on topographically patterned substrates in the presence of MMP3 inhibitor

In the absence of an EF, directedness of cell migration was not significantly different on planar vs. patterned surfaces and was similar in the presence or absence of 20 μM MMP3i. Greater cell migration rate was observed on stochastic surfaces in comparison with planar surfaces (data not shown). In the absence of an EF,

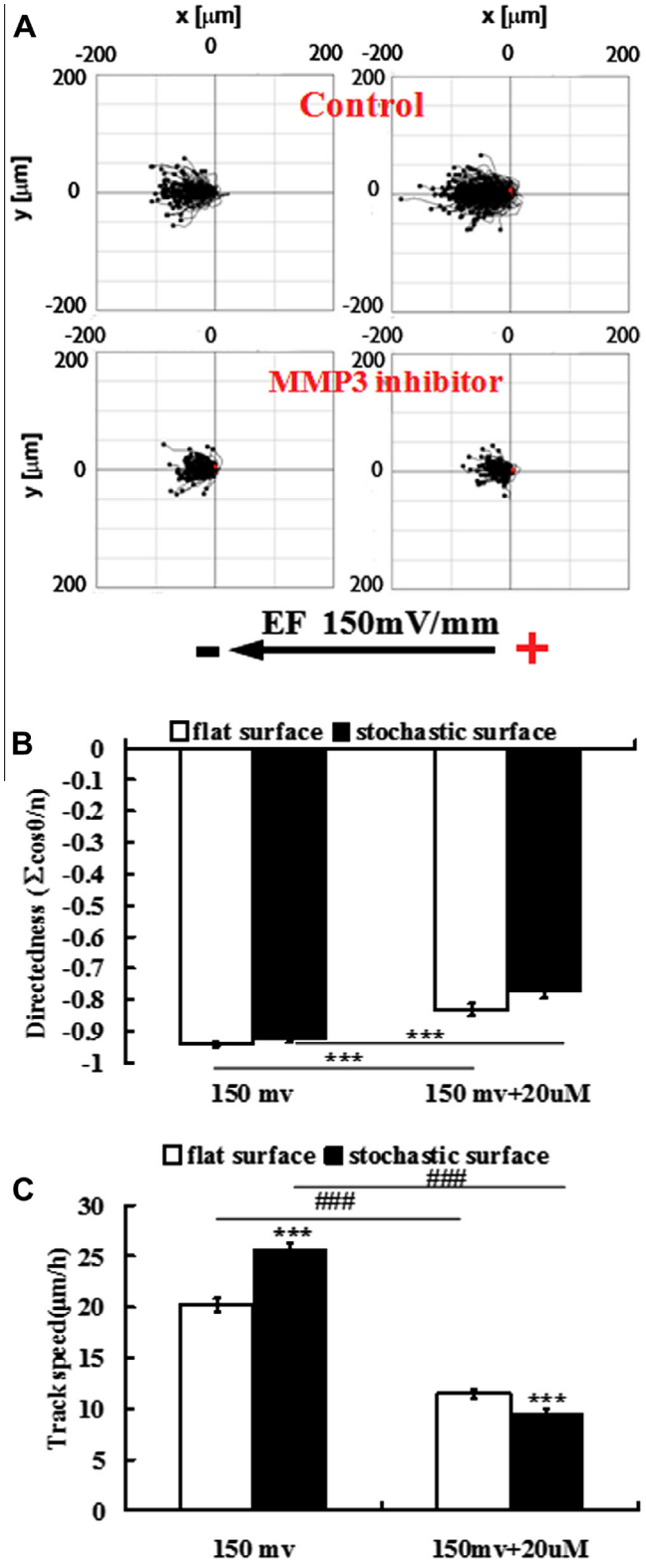

Fig. 6. Synergistic enhancement of cell migration by EFs and stochastic topography was mediated by MMP3. (A) Cell tracks show reduced migration rate in EF on both flat and stochastic surfaces in the presence of MMP3 inhibitor (MMP3i). (B) Quantification of cell migration showed that cell directionality in 20 μM MMP3i was impaired. This impairment was greater on stochastic than on flat surfaces. (C) Cell migration speed was dramatically reduced in MMP3i, especially on stochastic surfaces. Results are mean ± standard error; Mann–Whitney rank sum test, $^{***}P < 0.001$ are results comparing stochastic surfaces with planar surfaces for each treatment; $^{\#\#\#}P < 0.001$ are results comparing MMP3i treated cells with control cultures on respective surfaces.

migration rate on planar and topographically patterned surfaces was unaffected by the presence of 20 μM MMP3i. In contrast, treatment of cells with 20 μM MMP3i had significant phenotypic consequences on cell migration when a 150 mV mm^{-1} EF was applied (Fig. 6). Specifically, directed migration of single cells was impaired in the presence of MMP3i and impairment was exacerbated on patterned surfaces (Fig. 6A and B). Likewise, cell migration rates were significantly lower for those cultured on patterned surfaces in comparison with planar surfaces with the simultaneous presentation of both EF and MMP3i (Fig. 6C).

3.5. Migration of cells from a confluent monolayer

We noticed differences in cell behavior on stochastically patterned surfaces vs. flat when the cells were grown to confluence and allowed to migrate into a cell-free analytic zone. Cells on planar surfaces spread out and migrated individually, whereas cells on patterned surfaces stayed together and migrated as a unified sheet (Fig. 7A and Supplementary movies 5 and 6). We analyzed cell migration by measuring the distance between adjacent pairs of cells across the "wound space" at time zero and 3 h after stopper removal. Confluent cells on patterned surfaces remained cohesive and migrated collectively, whereas cells on planar surfaces dissociated from the confluent monolayer to migrate individually (Fig. 7B). Migration rates, although presented in Fig. 7C should be compared taking into consideration that monolayer cell migration vs. single-cell migration on patterned vs. planar surfaces were observed, respectively.

4. Discussion

CECs are exposed simultaneously to a variety of biochemical, topographical and electrical cues in vivo. The corneal BM, by which CECs attach to the underlying stroma in vivo, possesses a rich 3-D stochastically organized nanoscale topography comprised of ECM proteins [16,18,46]. Biomimetic topographic cues have been documented to modulate a wide menu of CEC behaviors important to wound healing, including adhesion, migration and proliferation [6,39,47]. CECs migrate across the BM while being exposed to numerous soluble cytoactive factors and endogenous EFs. Natural EFs arise spontaneously upon wounding of many tissues, including epithelia, and are necessary for normal healing [48–50]. Wound electrical activity is a long-lasting response, and enhancing or inhibiting this electric signal increases or decreases wound healing, respectively [49]. Cells responsible for wound healing such as CECs or skin keratinocytes migrate directionally in EFs of physiological magnitude [31]. To our knowledge, there have been no prior published reports investigating the simultaneous influence of natural EFs and biologically and anatomically relevant topographic cues, both potent cues that impact epithelial cell behaviors during wound healing. In our studies, migration rate was significantly elevated when cells were cultured on topographically patterned substrates in comparison with planar surfaces, both in the presence or absence of an applied EF. A similar increase in migration rate has been reported in endothelial cells cultured on biomimetic stochastic surfaces [38]. The mechanisms underlying substratum-mediated elevated migration-rate remain poorly understood.

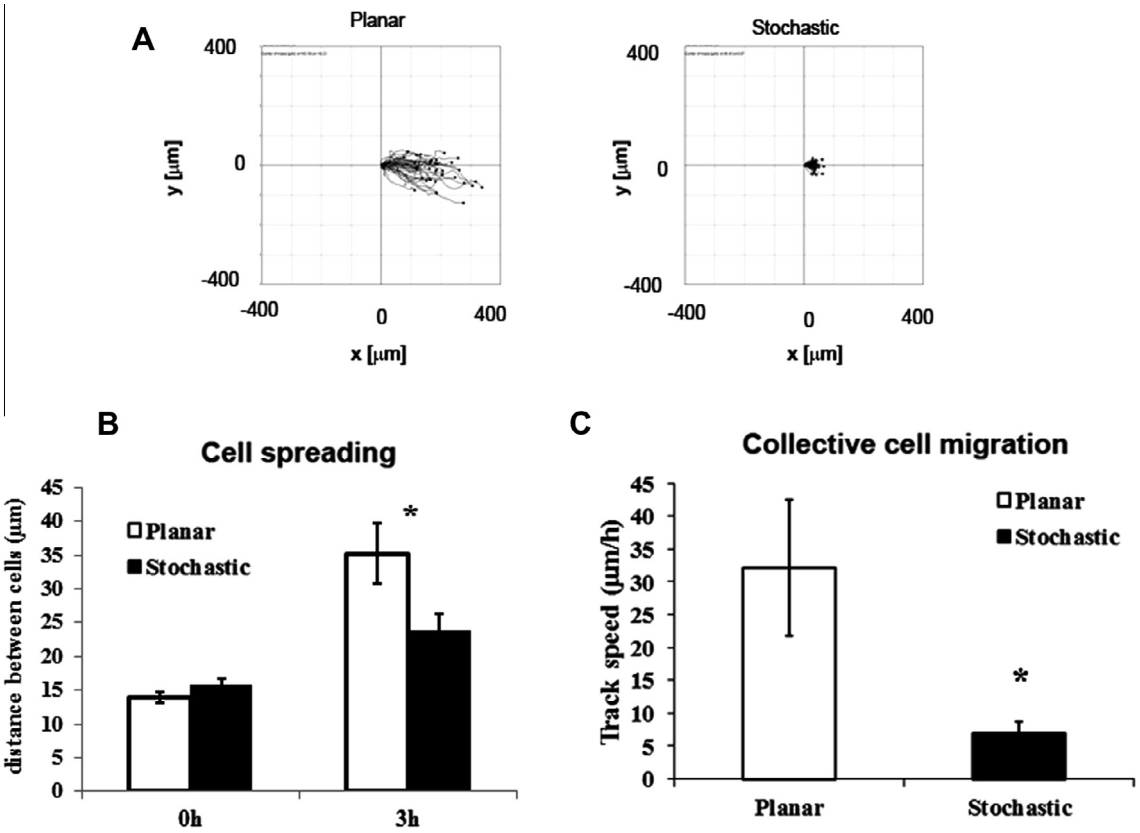

Fig. 7. Stochastically patterned surfaces facilitate cell migration as a sheet in the presence of an EF. (A) Cell tracks show single-cell migration on planar surfaces and migration of a confluent cell-monolayer on stochastic surfaces. (B) 3 h after the application of an EF, a greater distance between adjacent cells indicated dissociated cell migration on planar surfaces, while the distance between cells was lesser on stochastic surfaces. Results are mean ± standard error; *t*-test, $^{*}P < 0.05$ in comparison with planar surfaces. (C) Apparent cell migration rates of cohesive cell monolayers on stochastic surfaces are significantly lower than single-cell migration on planar surfaces. Results are mean ± standard deviation; *t*-test, $^{*}P < 0.05$ in comparison with planar surfaces.

MMPs are a family of extracellular enzymes that facilitate cell migration by breaking down localized collagen or matrix proteins allowing for turnover of the ECM. Additionally, MMPs are capable of impacting the microenvironment of migrating cells by acting on chemokines, cytokines, surface receptors and proteins [51–54]. The differing roles of various MMPs in epithelial repair and migration have been recently reviewed [55]. For example, MMP1 was demonstrated to be crucial for CEC migration when stimulated by soluble growth factors (hepatocyte growth factor) [56]; the modulation of MMP expression and activation by biophysical cues is not known. While MMP9 and MMP2 are most widely reported in wound healing of the skin and cornea, few studies have reported the role of MMP3 in wound healing. Mice lacking MMP3 demonstrated impaired skin wound contraction [57], and weak and transient localization of MMP3 was observed in the anterior stroma of rabbit corneas 3–7 days after anterior keratectomy. The exact role(s) of MMP3 in epithelial migration and repair remains poorly defined.

CECs in the presence of EFs demonstrated no change in gene expression of MMPs implicated in epithelial wound healing (MMP2, MMP9). Nevertheless, Rho- and Cdc42-mediated directional cell migration in the presence of an applied EF has previously been reported in bovine CECs [32]. In the present study, a 2-fold increase in MMP3 gene expression was observed in these CECs after application of EF. Secondary validation by Western blotting and immunocytochemistry conclusively verified elevated protein expression. This was accompanied by a concurrent increase in MMP3 activity in the media supernatant, indicating that stimulation of cells by EF resulted in secretion of MMP3 allowing for ECM turnover to facilitate cell migration. Indeed, in the presence of EF, cell migration was significantly faster than without EF.

Interestingly, in the presence of the strongest EF (150 mV mm^{-1}), MMP3 expression in cells, as well as activity in the cell-culture medium, were more elevated when cells were plated on topographically patterned surfaces in comparison with planar surfaces having the same surface chemistry. This result indicates that biomimetic substratum topography acted synergistically with applied EF in increasing MMP3 expression and activity. This may perhaps suggest that a threshold could exist that could bring about maximal responses when simultaneous biophysical cues are presented. Further studies will be required to delineate this phenomenon conclusively. To investigate the role of MMP3 in cell migration, we inhibited MMP3 activity in cells using a commercially available small molecule compound. Neither migration nor directness was significantly affected in the absence of EF (data not shown). However, in the presence of applied EFs, migration rate and directedness of cells were both strongly reduced when treated with MMP3 inhibitor. Intriguingly, stochastic topography exaggerated the extent of attenuation for both migration direction and speed. In aggregate, these data suggest topographic cues and EFs cause an acceleration in migration that is at least partially mediated through MMP3 activity. However, the interplay between gene and protein expression, and enzyme activity for the various MMPs, with the simultaneous presence of EFs and substratum biophysical cues, appears to be complex and requires further investigation. The specific roles of tissue inhibitor of metalloproteinase in MMP-EF mediated cell migration will be the subject of future studies.

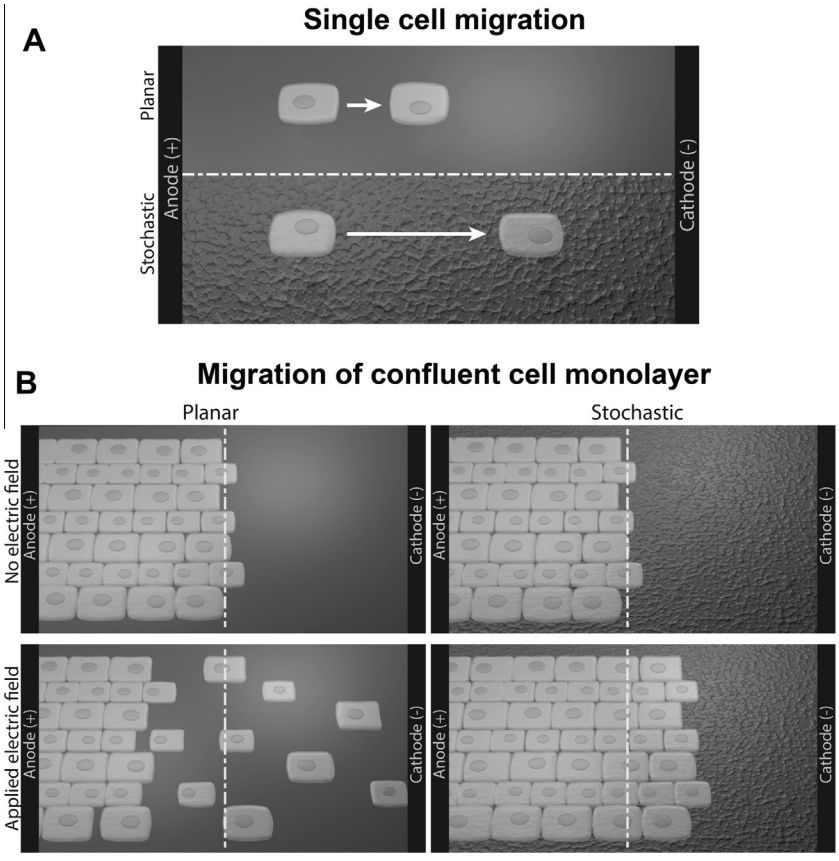

Fig. 8. Schematic representation of the simultaneous effect of stochastic topography and applied EF on single and collective cell migration. (A) In the presence of an applied EF, single cells cultured on stochastically patterned surfaces migrate towards the cathode significantly faster than those cultured on chemically identical planar surfaces. (B) When cultured as a confluent sheet, cells cultured on stochastically patterned surfaces migrate collectively as one would expect in a wound in vivo. In comparison, cells migrated as single cells on planar surfaces despite being cultured as a confluent sheet.

Re-establishment of the BM is one of the critical events that occur during corneal wound healing. Collective migration of CECs as a sheet occurred when cultured as a monolayer on topographically patterned surfaces in the presence of an applied EF, whereas cells dissociated from the wound margin and migrated individually into the wound space when cells were cultured on planar surfaces. This finding suggests that biomimetic topographic cues facilitate wound closure as a sheet. While further studies are required to examine the underlying mechanism(s) for this effect, we feel it likely that stochastic topographic cues promote increased intercellular adhesions. It is well documented that anisotropic topographic cues modulate single-cell–substrate adhesion [6]. The extent to which cell–substrate and cell–cell adhesion is altered on stochastically patterned surfaces when cultured as a monolayer is yet to be determined.

Although the results suggest that migration of confluent cells is slower than single-cell migration, such comparisons ought to be made in light of the crucial differences in migratory patterns. When cultured as a confluent layer and in the presence of an applied EF, on cells planar surfaces dissociated from the "wound" margin and migrated as single cells. In contrast, on stochastically patterned surfaces, cells were cohesive and migrated collectively as one would observe in a wound in vivo. Thus comparing the migratory rates directly should be approached cautiously. However, this result is most interesting in light of recent work showing that cells in sheets or groups are much more sensitive to applied EFs than individual cells [58]. This result is particularly relevant in highlighting the importance of the BM-like features and biophysical stimuli when evaluating the efficacy of drugs/cytoactive factors that promote cell migration/wound closure. Results presented in this study demonstrate that CECs are more responsive to an EF on a biomimetic topographical substrate and MMP3 may play a significant role in facilitating CEC migration.

5. Conclusions

Human CECs migrated towards the cathode in the presence of an EF on both flat and nanopatterned surfaces. Because cells migrated significantly faster on stochastically patterned biomimetic surfaces mimicking the BM, this finding may be exploited for engineering novel strategies to promote corneal wound healing. While the molecular mechanisms responsible for the interaction between EFs and topographic cues are not yet clear, our study highlights the importance of presentation of simultaneous yet biologically relevant cues to study corneal wound healing processes, and that MMPs may play a significant role in the regulation of EF-mediated directional cell migration. This is in stark contrast to the flat hard surfaces of tissue culture plastic used in most in vitro investigations. A summary of the findings reported here is illustrated as a schematic in Fig. 8. In the proposed model, we suggest that an EF enhances single-cell migration to a greater extent on stochastically patterned surfaces. In addition, when cells are cultured as a confluent sheet and in the presence of an applied EF, the underlying biomimetic topography promotes collective cell migration rather than single-cell movement, which is a characteristic of corneal epithelial wound closure in vivo.

Acknowledgments

This work is supported by grants from the National Institute of Health (1R01EY019101, R01EY016134, NSF [MCB-0951199], R01 EY019970 and P30 EY12576), Province Talented Recruiting Program [2009CI127], the National Basic Research Program of China (973 Program) 2012CB518105, National Science Foundation of China [U1132603], and an unrestricted grant from Research to Prevent Blindness. We are grateful to Dr. James V. Jester (UC Irvine) for providing the hTCEpi cells. The authors thank Mr. John Doval for his assistance with the preparation of graphics.

Appendix A. Figures with essential colour discrimination

Certain figures in this article, particularly Figures 1, 2, 5 and 6 are difficult to interpret in black and white. The full colour images can be found in the on-line version, at http://dx.doi.org/10.1016/j.actbio.2014.10.007.

Appendix B. Supplementary data

Supplementary data associated with this article can be found, in the online version, at http://dx.doi.org/10.1016/j.actbio.2014.10.007.

References

[1] Suzuki K, Tanaka T, Enoki M, Nishida T. Coordinated reassembly of the basement membrane and junctional proteins during corneal epithelial wound healing. Invest Ophthalmol Vis Sci 2000;41:2495–500.
[2] Yu FSX, Yin J, Xu K, Huang J. Growth factors and corneal epithelial wound healing. Brain Res Bull 2010;81:229–35.
[3] Chi C, Trinkaus-Randall V. New insights in wound response and repair of epithelium. J Cell Physiol 2013;228:925–9.
[4] Raghunathan VK, McKee CT, Tocce EJ, Nealey PF, Russell P, Murphy CJ. Nuclear and cellular alignment of primary corneal epithelial cells on topography. J Biomed Mater Res A 2013;101:1069–79.
[5] Fraser SA, Ting Y-H, Mallon KS, Wendt AE, Murphy CJ, Nealey PF. Sub-micron and nanoscale feature depth modulates alignment of stromal fibroblasts and corneal epithelial cells in serum-rich and serum-free media. J Biomed Mater Res, Part A 2008;86A:725–35.
[6] Karuri NW, Liliensiek S, Teixeira AI, Abrams G, Campbell S, Nealey PF, et al. Biological length scale topography enhances cell-substratum adhesion of human corneal epithelial cells. J Cell Sci 2004;117:3153–64.
[7] Karuri NW, Nealey PF, Murphy CJ, Albrecht RM. Structural organization of the cytoskeleton in SV40 human corneal epithelial cells cultured on nano- and microscale grooves. Scanning 2008;30:405–13.
[8] Karuri NW, Porri TJ, Albrecht RM, Murphy CJ, Nealey PF. Nano- and microscale holes modulate cell-substrate adhesion, cytoskeletal organization, and -beta1 integrin localization in SV40 human corneal epithelial cells. IEEE Trans Nanobiosci 2006;5:273–80.
[9] Teixeira AI, McKie GA, Foley JD, Bertics PJ, Nealey PF, Murphy CJ. The effect of environmental factors on the response of human corneal epithelial cells to nanoscale substrate topography. Biomaterials 2006;27:3945–54.
[10] Tocce EJ, Broderick AH, Murphy KC, Liliensiek SJ, Murphy CJ, Lynn DM, et al. Functionalization of reactive polymer multilayers with RGD and an antifouling motif: RGD density provides control over human corneal epithelial cell-substrate interactions. J Biomed Mater Res A 2012;100:84–93.
[11] Tocce EJ, Liliensiek SJ, Broderick AH, Jiang Y, Murphy KC, Murphy CJ, et al. The influence of biomimetic topographical features and the extracellular matrix peptide RGD on human corneal epithelial contact guidance. Acta Biomater 2013;9:5040–51.
[12] Wilson MJ, Liliensiek SJ, Murphy CJ, Murphy WL, Nealey PF. Hydrogels with well-defined peptide-hydrogel spacing and concentration: impact on epithelial cell behavior. Soft Matter 2012;8:390–8.
[13] Raghunathan V, McKee CT, Cheung W, Naik R, Nealey PF, Russell P, et al. Influence of extracellular matrix proteins and substratum topography on corneal epithelial cell alignment and migration. Tissue Eng Part A 2013.
[14] Liliensiek SJ, Nealey P, Murphy CJ. Characterization of endothelial basement membrane nanotopography in rhesus macaque as a guide for vessel tissue engineering. Tissue Eng Part A 2009;15:2643–51.
[15] Abrams GA, Bentley E, Nealey PF, Murphy CJ. Electron microscopy of the canine corneal basement membranes. Cells Tissues Organs 2002;170:251–7.
[16] Abrams GA, Goodman SL, Nealey PF, Franco M, Murphy CJ. Nanoscale topography of the basement membrane underlying the corneal epithelium of the rhesus macaque. Cell Tissue Res 2000;299:39–46.
[17] Abrams GA, Murphy CJ, Wang ZY, Nealey PF, Bjorling DE. Ultrastructural basement membrane topography of the bladder epithelium. Urol Res 2003;31:341–6.
[18] Abrams GA, Schaus SS, Goodman SL, Nealey PF, Murphy CJ. Nanoscale topography of the corneal epithelial basement membrane and descemet's membrane of the human. Cornea 2000;19:57–64.
[19] Hironaka K, Makino H, Yamasaki Y, Ota Z. Renal basement membranes by ultrahigh resolution scanning electron microscopy. Kidney Int 1993;43:334–45.

[20] Inoue S. Basic structure of basement membranes is a fine network of "cords", irregular anastomosing strands. Microsc Res Tech 1994;28:29–47.
[21] Whittaker ET. The classical theories. 2nd ed. London: Nelson; 1951.
[22] Roux W. Uber die morphologische Polarisation von Eiern und Embryonen durch den electrischen Strom etc.. Sitzungsber Acad Wiss Wien, Math Naturwiss Kl 1892;101:27–228.
[23] Jaffe LF, Poo MM. Neurites grow faster towards the cathode than the anode in a steady field. J Exp Zool 1979;209:115–28.
[24] Hinkle L, McCaig CD, Robinson KR. The direction of growth of differentiating neurons and myoblasts from frog embryos in an applied electric field. J Physiol 1981;314:121–35.
[25] Stump RF, Robinson KR. Xenopus neural crest cell migration in an applied electrical field. J Cell Biol 1983;97:1226–33.
[26] Erickson CA, Nuccitelli R. Embryonic fibroblast motility and orientation can be influenced by physiological electric fields. J Cell Biol 1984;98:296–307.
[27] Cooper MS, Schliwa M. Electrical and ionic controls of tissue cell locomotion in DC electric fields. J Neurosci Res 1985;13:223–44.
[28] Farboud B, Nuccitelli R, Schwab IR, Isseroff RR. DC electric fields induce rapid directional migration in cultured human corneal epithelial cells. Exp Eye Res 2000;70:667–73.
[29] Zhao M, McCaig CD, Agius-Fernandez A, Forrester JV, Araki-Sasaki K. Human corneal epithelial cells reorient and migrate cathodally in a small applied electric field. Curr Eye Res 1997;16:973–84.
[30] Nishimura KY, Isseroff RR, Nuccitelli R. Human keratinocytes migrate to the negative pole in direct current electric fields comparable to those measured in mammalian wounds. J Cell Sci 1996;109(Pt 1):199–207.
[31] Zhao M, Agius-Fernandez A, Forrester JV, McCaig CD. Directed migration of corneal epithelial sheets in physiological electric fields. Invest Ophthalmol Vis Sci 1996;37:2548–58.
[32] Rajnicek AM, Foubister LE, McCaig CD. Alignment of corneal and lens epithelial cells by co-operative effects of substratum topography and DC electric fields. Biomaterials 2008;29:2082–95.
[33] Zhao M. Electrical fields in wound healing – an overriding signal that directs cell migration. Semin Cell Dev Biol 2009;20:674–82.
[34] Reid B, Song B, McCaig CD, Zhao M. Wound healing in rat cornea: the role of electric currents. FASEB J 2005;19:379–86.
[35] Chiang M, Robinson KR, Vanable JW. Electrical fields in the vicinity of epithelial wounds in the isolated bovine eye. Exp Eye Res 1992;54:999–1003.
[36] Nuccitelli R, Nuccitelli P, Ramlatchan S, Sanger R, Smith PJS. Imaging the electric field associated with mouse and human skin wounds. Wound Repair Regen 2008;16:432–41.
[37] Robertson DM, Li L, Fisher S, Pearce VP, Shay JW, Wright WE, et al. Characterization of growth and differentiation in a telomerase-immortalized human corneal epithelial cell line. Invest Ophthalmol Vis Sci 2005;46:470–8.
[38] McKee CT, Wood JA, Ly I, Russell P, Murphy CJ. The influence of a biologically relevant substratum topography on human aortic and umbilical vein endothelial cells. Biophys J 2012;102:1–10.
[39] Liliensiek SJ, Campbell S, Nealey PF, Murphy CJ. The scale of substratum topographic features modulates proliferation of corneal epithelial cells and corneal fibroblasts. J Biomed Mater Res A 2006;79:185–92.
[40] Liliensiek SJ, Wood JA, Yong J, Auerbach R, Nealey PF, Murphy CJ. Modulation of human vascular endothelial cell behaviors by nanotopographic cues. Biomaterials 2010;31:5418–26.
[41] McKee Clayton T, RaghunathanVijay K, Nealey Paul F, Russell P, Murphy Christopher J. Topographic modulation of the orientation and shape of cell nuclei and their influence on the measured elastic modulus of epithelial cells. Biophys J 2011;101:2139–46.
[42] Zhao M, Agius-Fernandez A, Forrester JV, McCaig CD. Orientation and directed migration of cultured corneal epithelial cells in small electric fields are serum dependent. J Cell Sci 1996;109(Pt 6):1405–14.
[43] Song B, Gu Y, Pu J, Reid B, Zhao Z, Zhao M. Application of direct current electric fields to cells and tissues in vitro and modulation of wound electric field in vivo. Nat Protoc 2007;2:1479–89.
[44] Raghunathan VK, Morgan JT, Dreier B, Reilly CM, Thomasy SM, Wood JA, et al. Role of substratum stiffness in modulating genes associated with extracellular matrix and mechanotransducers YAP and TAZ. Invest Ophthalmol Vis Sci 2013;54:378–86.
[45] Schneider CA, Rasband WS, Eliceiri KW. NIH image to ImageJ: 25 years of image analysis. Nat Methods 2012;9:671–5.
[46] Abrams GA, Bentley E, Nealey PF, Murphy CJ. Electron microscopy of the canine corneal basement membranes. Cells Tissues Organs 2002;170:251–7.
[47] Diehl KA, Foley JD, Nealey PF, Murphy CJ. Nanoscale topography modulates corneal epithelial cell migration. J Biomed Mater Res, Part A 2005;75A:603–11.
[48] Zhao M, Song B, Pu J, Wada T, Reid B, Tai G, et al. Electrical signals control wound healing through phosphatidylinositol-3-OH kinase-gamma and PTEN. Nature 2006;442:457–60.
[49] Reid B, Song B, McCaig CD, Zhao M. Wound healing in rat cornea: the role of electric currents. FASEB J 2005;19:379–86.
[50] Reid B, Nuccitelli R, Zhao M. Non-invasive measurement of bioelectric currents with a vibrating probe. Nat Protoc 2007;2:661–9.
[51] Li Q, Park PW, Wilson CL, Parks WC. Matrilysin shedding of syndecan-1 regulates chemokine mobilization and transepithelial efflux of neutrophils in acute lung injury. Cell 2002;111:635–46.
[52] McQuibban GA, Gong JH, Tam EM, McCulloch CA, Clark-Lewis I, Overall CM. Inflammation dampened by gelatinase A cleavage of monocyte chemoattractant protein-3. Science 2000;289:1202–6.
[53] Levi E, Fridman R, Miao HQ, Ma YS, Yayon A, Vlodavsky I. Matrix metalloproteinase 2 releases active soluble ectodomain of fibroblast growth factor receptor 1. Proc Natl Acad Sci USA 1996;93:7069–74.
[54] Wilson CL, Ouellette AJ, Satchell DP, Ayabe T, Lopez-Boado YS, Stratman JL, et al. Regulation of intestinal alpha-defensin activation by the metalloproteinase matrilysin in innate host defense. Science 1999;286:113–7.
[55] Chen P, Parks WC. Role of matrix metalloproteinases in epithelial migration. J Cell Biochem 2009;108:1233–43.
[56] Daniels JT, Limb GA, Saarialho-Kere U, Murphy G, Khaw PT. Human corneal epithelial cells require MMP-1 for HGF-mediated migration on collagen I. Invest Ophthalmol Vis Sci 2003;44:1048–55.
[57] Bullard KM, Lund L, Mudgett JS, Mellin TN, Hunt TK, Murphy B, et al. Impaired wound contraction in stromelysin-1-deficient mice. Ann Surg 1999;230:260–5.
[58] Li L, Hartley R, Reiss B, Sun Y, Pu J, Wu D, et al. E-cadherin plays an essential role in collective directional migration of large epithelial sheets. Cell Mol Life Sci 2012;69:2779–89.